Vibrational relaxation in simulated two-dimensional infrared spectra of two amide modes in solution

Dijkstra, Arend G.; Jansen, Thomas la Cour; Bloem, Robbert; Knoester, Jasper

Published in:
Journal of Chemical Physics

DOI:
10.1063/1.2786455

Publication date:
2007

Vibrational relaxation in simulated two-dimensional infrared spectra of two amide modes in solution

Arend G. Dijkstra, Thomas la Cour Jansen, Robbert Bloem, and Jasper Knoester[a)]
Centre for Theoretical Physics and Zernike Institute for Advanced Materials, University of Groningen, Nijenborgh 4, 9747 AG Groningen, The Netherlands

(Received 12 July 2007; accepted 28 August 2007; published online 21 November 2007)

Two-dimensional infrared spectroscopy is capable of following the transfer of vibrational energy between modes in real time. We develop a method to include vibrational relaxation in simulations of two-dimensional infrared spectra at finite temperature. The method takes into account the correlated fluctuations that occur in the frequencies of the vibrational states and in the coupling between them as a result of interaction with the environment. The fluctuations influence the two-dimensional infrared line shape and cause vibrational relaxation during the waiting time, which is included using second-order perturbation theory. The method is demonstrated by applying it to the amide-I and amide-II modes in *N*-methylacetamide in heavy water. Stochastic information on the fluctuations is obtained from a molecular dynamics trajectory, which is converted to time dependent frequencies and couplings with a map from a density functional calculation. Solvent dynamics with the same frequency as the energy gap between the two amide modes lead to efficient relaxation between amide-I and amide-II on a 560 fs time scale. We show that the cross peak intensity in the two-dimensional infrared spectrum provides a good measure for the vibrational relaxation. © *2007 American Institute of Physics*. [DOI: 10.1063/1.2786455]

I. INTRODUCTION

The flow of energy in biomolecules through vibrational relaxation is a much-studied topic.[1–4] Energy is released into vibrational modes somewhere in a protein, for example, by hydrolysis of adenosine triphosphate (ATP). This energy then disappears into other vibrational modes, where it can be used to drive chemical reactions. In particular the amide-I mode is expected to play a role in the energy transport.[1] The relaxation process from initially excited amide-I vibrations occurs very fast, typically on a picosecond time scale.[5] To gain a more precise understanding of the energy transport, it is of interest to study the ultrafast relaxation pathways that play a role in the decay of the amide-I mode.

Two-dimensional infrared (2DIR) spectroscopy is well suited for studying such vibrational relaxation in biomolecules. In the 2DIR experiment, two initial ultrafast laser pulses are used to excite (coherent superpositions of) vibrational states. The excited system is then left to evolve freely during a waiting time, after which its state is probed. Spectra are plotted as a two-dimensional map correlating the initially excited state with the final state. The 2DIR technique has been applied to proteins in solution.[5–10] However, most studies have focused on spectra with zero waiting time. Using the waiting time dependence gives a direct way to study system dynamics, including population relaxation. The two-dimensional line shape is determined by bath-induced fluctuations in the energy of the excited state, and therefore gives statistical information on these fluctuations as a function of the waiting time.[11] Information on the interaction between two modes can be obtained from cross peaks. If the energy difference between two vibrational modes is smaller than the bandwidth of the applied laser pulses, they can be excited coherently. In this case, cross peaks give direct information on the interaction.[12] The shape of the cross peak, in particular tilting away from the horizontal, contains information about correlations in the frequencies of the two modes that form the cross peak.[13]

On the theory side, much work remains to be done before accurate quantitative comparisons with experimental 2DIR spectra can be made. Different methods have been used to simulate 2DIR spectra,[14–17] again, mostly for zero waiting time. In particular, the inclusion of vibrational relaxation in the simulation of 2DIR spectra has received little attention.

Conceptually the simplest picture used to simulate spectra starts from a static description of vibrational modes. Two different methods have been used that proceed along these lines. The most straightforward is the sum over states approach.[5,18,19] Fluctuations of spectroscopic parameters are often treated in the Bloch limit, where slow and fast dynamics are clearly separated. Fast fluctuations are included by replacing the frequency-frequency autocorrelation function of a vibrational mode with a delta peak at zero time. This leads to Lorentzian lines in the spectrum. The slow fluctuations can then be added as a constant term in the correlation function. This effect—also called static disorder—can be handled by Monte Carlo sampling, where the spectra of different realizations of the disorder are summed.[5,18,19] The nonlinear exciton equations[20] are a more advanced way to calculate the nonlinear response using less computer time, by

[a)]Electronic mail: j.knoester@rug.nl

replacing anharmonicity with scattering between excitons. Like the sum over states approach, the nonlinear exciton equations are limited to Bloch dynamics.

The above descriptions give an entirely static picture of the vibrational states. In reality, in a protein in solution at room temperature, all system parameters are fluctuating wildly on different time scales. Hence, the Bloch limit is not generally applicable. In addition, nonlinear optical experiments can explicitly probe the time evolution of system parameters during the waiting time. To describe these experiments correctly, we need to take into account the time dependence explicitly.

More sophisticated ways to calculate spectra that are capable of treating fluctuations on different time scales are the stochastic approach[16] and the cumulant expansion.[21,22] The former method is well suited for the treatment of strong system-bath coupling. The frequency fluctuations resulting from strong coupling are comparable to or larger than the energy separation between modes, and using the stochastic method they can systematically be included in a nonperturbative way. The price that has to be paid for this high accuracy is the expensive numerical implementation. Fluctuations with arbitrary correlation function can also be treated in the cumulant expansion, which is exact as long as the fluctuations are Gaussian. However, vibrational relaxation is not included in this approach.

Numerical integration of the Schrödinger equation[14,23,24] has been applied to calculate 2DIR spectra as a function of the waiting time. In principle, this method is able to account for dynamics on all time scales, as well as relaxation. This method implicitly assumes infinite temperature: after a long waiting time the populations of all states in the system will be the same. The method thus gives a correct description for relaxation between states that are separated in energy by less than the thermal energy kT, but is less accurate if the energy separation is comparable to or larger than kT. In practice, while the method works very well for small systems, it is computationally demanding and thus hard to apply to larger systems.

It is the goal of this paper to include relaxation between different vibrational modes in the calculations of 2DIR spectra. We describe a theory of relaxation at finite temperature and the simulation protocol used to include this theory in the calculation of 2DIR spectra.

We then demonstrate our approach by applying it to *N*-methylacetamide (NMA) in heavy water, where the hydrogen in the amide group is replaced by deuterium. NMA has been widely studied as a small model compound containing one amide group.[12,25–33] Because of its large infrared intensity, most interest has focused on the amide-I mode, a vibration that is dominated by the C=O stretch motion. It has a frequency of 1600–1700 cm^{-1},[12] depending on the solvent. The mode closest in energy below the amide-I is the amide-II mode, a C–N stretch combined with C–N–D bend (see Fig. 1), with a frequency 100–150 cm^{-1} lower than the amide-I. The energy gap between these two modes is comparable to the thermal energy (200 cm^{-1} at 300 K), so if relaxation occurs the excess energy can easily be dissipated in thermally populated modes. The amide-I and amide-II modes will inevitably be coupled by fluctuations in the environment. Therefore, it is natural to expect that relaxation between the amide-I and amide-II modes is efficient. This vibrational relaxation was studied experimentally by DeFlores *et al.*,[12] who measured linear and 2DIR spectra from coherent excitation of the two modes. They found strong interactions between the two modes and argued that the relaxation process between them shows rapid coherent exchange.

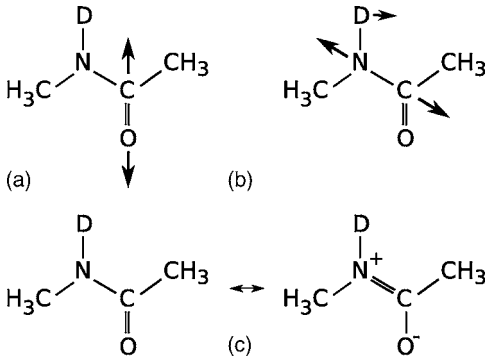

FIG. 1. Illustration of the atom movement in the (a) amide-1 and (b) amide-2 modes and the dominant resonance structure (c) in NMA (Ref. 45).

Fujisaki *et al.*[28] modeled vibrational relaxation from the amide-I mode of NMA in heavy water, using a sophisticated non-Markovian model. They tabulated nine different pathways that distribute energy to combinations of modes with frequencies between 550 and 1130 cm^{-1}. However, they found no relaxation to amide-II, because low-energy modes ($\omega < 300$ cm^{-1}) that can accept the excess energy were not treated in their model. Hayashi *et al.*[26,27] performed extensive simulations of NMA in normal water. They described the fluctuating frequency of, among others, the amide-I and amide-II modes, including correlations. 2DIR spectra were calculated using the cumulant expansion. Vibrational relaxation and waiting time dependence were therefore not included.

In the following sections, we will first describe the model used to simulate spectra (Sec. II), followed by the theory of vibrational relaxation (Sec. III). In Sec. IV we discuss the fluctuating Hamiltonian for the amide-I and amide-II modes in NMA (Sec. IV A), the resulting vibrational redistribution and the infrared spectra (Sec. IV B). We conclude in Sec. V. The Appendix explains the generation of correlated Gaussian random processes needed in the simulation of 2DIR spectra.

II. THEORY: SPECTROSCOPY

Fluctuations in vibrational frequencies and relaxation processes can be studied using infrared spectroscopy. Linear absorption spectra show the effect of fluctuating frequencies through the spectral line shape. Information on vibrational relaxation cannot be obtained directly from a linear spectrum. Much more information on dynamics is obtained from the 2DIR experiment. In the 2DIR spectrum, the initial frequency of an oscillator is correlated with its frequency after a certain waiting time. A 2DIR experiment is performed with three or four short laser pulses. The first pulse excites a coherent superposition of states containing one vibrational

quantum and the ground state. After a time t_1, a second pulse is applied, which is followed by the waiting time. During this time, which will also be called t_2, the system is either in a population of a one-quantum state or in a coherence between two one-quantum states. Finally, a time t_3 follows the third pulse and an observable third-order signal is radiated from a coherent superposition of a one-quantum state and the ground state or of a one- and a two-quantum state. During all of these three times, fluctuations in the frequencies and in the interactions between modes take place. These fluctuations influence the line shape that is observed in the 2DIR spectrum and cause relaxation processes between the states. Because the waiting time can be varied experimentally, 2DIR spectroscopy provides a direct probe of the fluctuations during this time.

From a model viewpoint, the (quantum mechanical) description of a spectroscopic experiment on a protein in a solvent starts from a Hamiltonian. The Hamiltonian must include all relevant vibrational states in the protein and in the solvent, as well as the interactions between these states and with the applied electromagnetic field. On the basis of their visibility in the spectrum, the set of vibrations can be split into two parts called system and bath. The system consists of the modes that are coupled to the electromagnetic field directly. In an infrared experiment, these are the modes with a significant oscillator strength in the infrared region and an excitation energy within the pulse bandwidth. All other modes form the bath. Because a typical experiment probes a few system modes that are coupled to many bath modes, it is advantageous to use a reduced description of the spectra in terms of system modes only. The Hamiltonian can then be written down as a matrix in a chosen fixed basis, in our approach containing the gas-phase normal modes. Diagonal Hamiltonian matrix elements are the frequencies of the modes which form the basis set and off-diagonal elements denote interactions between them. Even though the normal modes are noninteracting in the gas phase, the average off-diagonal matrix elements are nonzero in solution. In a static situation, one would then choose the basis such that the interactions are zero. However, because of the coupling between system and bath modes, the matrix elements of the Hamiltonian in a reduced description fluctuate in time and time-varying interactions appear. These fluctuations are responsible for vibrational relaxation. One of the relaxation effects is population redistribution. Population that is initially in one vibrational mode is redistributed over all available modes until equilibrium is reached. The time scale of the relaxation process is determined by the frequencies and amplitudes of the fluctuations. Thus, with a suitable method, it is possible to simulate vibrational relaxation from the knowledge of the fluctuations.

In the fixed reduced basis of system states, we label the system modes by an index n. Their bosonic creation and annihilation operators are denoted by $b_n^\dagger$ and b_n, respectively. The mode anharmonicity is denoted by A_n. Bath modes are labeled by the index x, their bosonic operators are denoted $a_x^\dagger$ and a_x; bath mode x has frequency ω_x. We assume that the bath modes are harmonic oscillators; they couple to the system modes with strength g^x. The total Hamiltonian is a sum of terms, $H_T=H_S+H_B+H_{SB}+H_{SL}$, which describe the system, the bath, the system-bath interaction, and the system-light interaction, respectively, and these terms are given by ($\hbar=1$),

$$H_S=\sum_{mn} H_{mn}b_m^\dagger b_n-\sum_n A_n b_n^\dagger b_n^\dagger b_n b_n, \tag{1}$$

$$H_B=\sum_x \left(\omega_x+\frac{1}{2}\right)a_x^\dagger a_x, \tag{2}$$

$$H_{SB}=\sum_{mn} b_m^\dagger b_n F_{mn}, \tag{3}$$

$$F_{mn}=\sum_x g_{mn}^x(a_x^\dagger+a_x), \tag{4}$$

$$H_{SL}=-\sum_m \boldsymbol{\mu}_m\cdot\tilde{\mathbf{E}}(t)(b_m^\dagger+b_m). \tag{5}$$

Labels m and n run over system states, which have energies H_{mm} and interact by bilinear couplings H_{mn}. H_{SB} accounts for the fluctuations in these quantities to first order in the bath coordinates. $\tilde{\mathbf{E}}$ is the applied electromagnetic field.

Under the assumption of weak incident fields, standard third-order perturbation theory can be used for the term H_{SL} to obtain the nonlinear response.[34,35] This response is given in terms of the total density matrix ϱ of the system plus the bath, which can be expanded in a basis of eigenstates of $H_S+H_B+H_{SB}$. As indicated previously, we wish to express the response in terms of the reduced density matrix σ of the system only. To obtain this description, we look at the equation of motion for the reduced density operator, which is given by[36]

$$i\dot{\sigma}(t)=[H_S,\sigma(t)]+\mathrm{tr}_B[H_{SB},\varrho(t)], \tag{6}$$

where the dot denotes the time derivative and tr_B is the trace over bath modes. This equation still contains a term with the full density matrix. To treat this term, we make a perturbative expansion in H_{SB}. This expansion will be to first order during t_1 and t_3, when the system is in a coherence, and to second order during t_2 to allow for population redistribution.

During the coherence times t_1 and t_3, we will assume that the system-bath coupling is constant. This is the static approximation for the system; the matrix elements of the Hamiltonian in the basis of system eigenstates are constant in time. To first order, the total density matrix factors into a direct product of the reduced density matrix and a bath part. The equation of motion for the reduced density operator then simply becomes[36]

$$i\dot{\sigma}(t)=[H_S+\langle H_{SB}\rangle+\Delta H(t),\sigma(t)]. \tag{7}$$

Here, $\langle H_{SB}\rangle+\Delta H(t)=\mathrm{tr}_B(H_{SB}\varrho(t))$ denotes the effect of the bath on the Hamiltonian in the reduced basis at time t. The average contribution is given by $\langle H_{SB}\rangle=\mathrm{tr}_B(H_{SB}\varrho_{\mathrm{eq}})$, where ϱ_{eq} is the equilibrium density operator. The shift from the average at time t is $\Delta H(t)=\Sigma_{mn}b_m^\dagger b_n\langle F_{mn}\rangle_t$, with matrix elements $\langle F_{mn}\rangle_t=\mathrm{tr}_B(F_{mn}(\varrho(t)-\varrho_{\mathrm{eq}}))$. Before the waiting time, and thus during t_1, the shifts are given by $\Delta H(0)$. Fluctua-

tions during the waiting time t_2 have the effect that the shifts after the waiting time, $\Delta H(t_2)$, are different from $\Delta H(0)$, although they can be correlated. We will denote the Hamiltonian including the effect of the bath as $H=H_S+\langle H_{SB}\rangle+\Delta H(0)$ during t_1 and as $H'=H_S+\langle H_{SB}\rangle+\Delta H(t_2)$ during t_3.

Thus, in this static approximation, the spectrum is averaged over realizations of the stochastic quantities $\Delta H(t)$. For each realization in the static average, we need to determine the matrix elements of $\Delta H(0)$ and $\Delta H(t_2)$ in the fixed basis. All these quantities are treated as correlated Gaussian random variables. Statistical relations between them are given by their correlation functions

$$C_{mnm'n'}(t)=\langle \Delta H_{mn}(\tau)\Delta H_{m'n'}(t+\tau)\rangle, \tag{8}$$

which only depend on the time difference t. For example, the cross-correlation function at time zero $C_{1122}(t=0)=\langle \Delta H_{11}(0)\Delta H_{22}(0)\rangle=\langle \Delta H_{11}(t_2)\Delta H_{22}(t_2)\rangle$ gives the correlation between H_{11} and H_{22} as well as between H'_{11} and H'_{22}. Correlation functions at nonzero time give relations between matrix elements of H and H'. As an example, the correlation between H_{11} and H'_{22} is given by a cross-correlation function at time t_2, $C_{2211}(t_2)=\langle \Delta H_{22}(t_2)\Delta H_{11}(0)\rangle$. Assuming that all auto- and cross-correlation functions for the frequencies and couplings are known, we use them to generate values for H_{mn} and H'_{mn} in each realization in the static average. This process is explained in the Appendix.

In a single realization, the constant Hamiltonian H during t_1 can be diagonalized to give eigenstates $|u\rangle$ and $|v\rangle$, with energies E_u and E_v. The first two laser pulses in the 2DIR experiment induce transitions between the ground state and these states. During t_3, the relevant states are eigenstates of H', and the one-quantum states are denoted $|u'\rangle$ and $|v'\rangle$. The third laser pulse can access states in the two-quantum manifold; these states are denoted $|w'\rangle$ and have energy $E_{w'}$. Transition dipoles between the ground state and a one-quantum eigenstate are denoted $\boldsymbol{\mu}_u$, $\boldsymbol{\mu}_{u'}$, etc. Dipoles $\boldsymbol{\mu}_{w'u'}$ between one- and two-quantum states are obtained from a harmonic approximation.[37] To complete the description of the 2DIR experiment, we need to connect the reduced density matrix in the t_1 basis of unprimed states to the reduced density matrix in the t_3 basis of primed states. Vibrational relaxation is included in this process. The connection is given by a time-dependent tensor $\mathcal{R}_{v'u'vu}(t_2)$, for which we will obtain an expression in Sec. III.

Following the standard time-dependent perturbation theory,[34,35] the calculation of the 2DIR spectra proceeds from the double-sided Feynman diagrams given in Fig. 2. The Feynman diagrams have been slightly modified from their standard form to show the relaxation during the waiting time. The waiting time is sliced into two parts by a dashed line. The indices below the line show the density matrix directly after the second pulse—before the relaxation process. Above the line is the state after relaxation, directly before the arrival of the third pulse. The 2DIR spectrum can then be calculated as the sum of the response from the six Feynman diagrams.

The three rephasing diagrams are the ground state bleach diagram, which gives a response

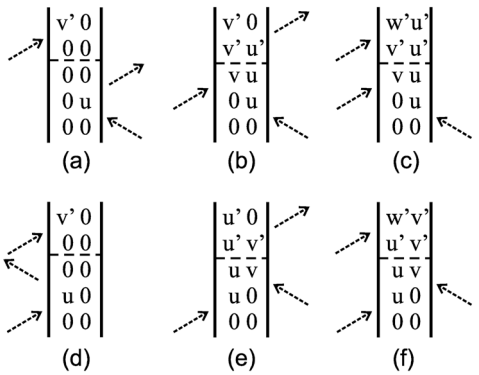

FIG. 2. The double-sided Feynman diagrams that contribute to the two-dimensional infrared signal. Diagram (a) rephasing ground state bleach, (b) rephasing stimulated emission, (c) rephasing induced absorption, (d) nonrephasing ground state bleach, (e) nonrephasing stimulated emission, and (f) nonrephasing induced absorption.

$$I^{\mathrm{GB}}(\omega_1,t_2,\omega_3)=A_{\alpha\beta\gamma\delta}\mu^{\delta}_{v'}\mu^{\gamma}_{v'}\mu^{\beta}_{u}\mu^{\alpha}_{u}\delta(\omega_1+E_u)\delta(\omega_3-E_{v'}), \tag{9}$$

the stimulated emission diagram,

$$I^{\mathrm{SE}}(\omega_1,t_2,\omega_3)=A_{\alpha\beta\gamma\delta}\mu^{\delta}_{v'}\mu^{\gamma}_{u'}\mathcal{R}_{v'u'vu}(t_2)\times\mu^{\beta}_{v}\mu^{\alpha}_{u}\delta(\omega_1+E_u)\delta(\omega_3-E_{v'}), \tag{10}$$

and the induced absorption diagram,

$$I^{\mathrm{IA}}(\omega_1,t_2,\omega_3)=-A_{\alpha\beta\gamma\delta}\mu^{\delta}_{w'u'}\mu^{\gamma}_{w'v'}\mathcal{R}_{v'u'vu}(t_2)\times\mu^{\beta}_{v}\mu^{\alpha}_{u}\delta(\omega_1+E_u)\delta(\omega_3-E_{w'}+E_{u'}). \tag{11}$$

For the nonrephasing diagrams, the response is

$$I^{\mathrm{GB}}(\omega_1,t_2,\omega_3)=A_{\alpha\beta\gamma\delta}\mu^{\delta}_{v'}\mu^{\gamma}_{v'}\mu^{\beta}_{u}\mu^{\alpha}_{u}\delta(\omega_1-E_u)\delta(\omega_3-E_{v'}), \tag{12}$$

$$I^{\mathrm{SE}}(\omega_1,t_2,\omega_3)=A_{\alpha\beta\gamma\delta}\mu^{\delta}_{u'}\mu^{\gamma}_{v'}\mathcal{R}_{u'v'uv}(t_2)\times\mu^{\beta}_{v}\mu^{\alpha}_{u}\delta(\omega_1-E_u)\delta(\omega_3-E_{u'}), \tag{13}$$

$$I^{\mathrm{IA}}(\omega_1,t_2,\omega_3)=-A_{\alpha\beta\gamma\delta}\mu^{\delta}_{w'v'}\mu^{\gamma}_{w'u'}\mathcal{R}_{u'v'uv}(t_2)\mu^{\beta}_{v}\mu^{\alpha}_{u}\times\delta(\omega_1-E_u)\delta(\omega_3-E_{w'}+E_{v'}). \tag{14}$$

Here, summations over the indices u, u', v, v', and w' are implied. $A_{\alpha\beta\gamma\delta}$ is the appropriate orientational coefficient for an arbitrary but given sequence of pulse polarizations (values can be found in Ref. 38), the four greek indices take values in $\{x,y,z\}$ and are also understood to be summed over.

In summary, in each realization in the static average, we construct energies and couplings of basis states during t_1, and different but correlated values during t_3, using the procedure outlined in the Appendix. The eigenstates resulting from these parameters are used in the calculation of the spectra. Populations in these eigenstates and coherent superpositions of states are connected by a relaxation procedure during the waiting time t_2. The total 2DIR spectrum is obtained as the

average over numerous realizations. The response from rephasing and nonrephasing pathways is summed to obtain absorptive 2DIR spectra.[11]

To conclude this section, we note that because the static approximation neglects fluctuations in time, the effect of motional narrowing is not present in our current approach. To remedy this, the effect could be included in a phenomenological way by averaging the correlation functions over a typical bath response time before using them in the calculations of spectra. The justification for this approach lies in the physical origin of motional narrowing as the inability of the system to repond to fluctuations that are faster than the typical response time. The averaging procedure removes the fastest dynamics, leading to an effective reduction of the amplitude of the fluctuations and thus narrower spectral lines.

III. THEORY: RELAXATION

To find an expression for the relaxation tensor $\mathcal{R}$, the dynamics during the waiting time t_2 need to be treated in more detail. During t_2, the system is either in a population of a one-quantum state or in a coherence between two different one-quantum states. The population will be redistributed over the one-quantum states because of the system-bath interaction. To describe the population redistribution during t_2, as well as the coupling between populations and coherences, we will go to the second order in the expansion in H_{SB} and make the Markoff approximation. This approach, leading to the Redfield equation is well known.[36,39,40] It is justified if the resulting relaxation times are slow compared to the energy level spacing and compared to the typical correlation times. In our application to the amide-I and amide-II modes in NMA (Sec. IV), we will find a relaxation time of 560 fs, while the level spacing corresponds to 300 fs and correlation functions decay with characteristic times between tens of femtoseconds and a few hundred femtoseconds (see Fig. 4).

We thus use the Redfield equation, which describes relaxation between eigenstates of the system Hamiltonian. However, in the present situation, we have to deal with the static shift of Hamiltonian matrix elements described in Sec. II. To account for this shift, we need to make a choice for the static part of the Hamiltonian during t_2. In each realization in the average we choose this static part to be

$$\tilde{H}_{mn} = H_{S,mn} + \langle H_{SB,mn} \rangle + \frac{1}{2}(\Delta H_{mn}(t_1) + \Delta H_{mn}(t_3)) \frac{C_{mnmn}(t_2)}{C_{mnmn}(0)}, \tag{15}$$

i.e., during a short waiting time t_2 each matrix element is the mean of its value during t_1 and t_3. For longer t_2 memory is lost, and the state of the system during t_1 and t_3 does not influence the relaxation process any longer. During t_2, we then express the reduced density matrix in terms of eigenstates of $\tilde{H}$ and calculate relaxation rates between these states caused by the fluctuations. The reduced density matrices in the basis of eigenstates of H and of $\tilde{H}$ are connected in the adiabatic approximation; i.e., the population in an eigenstate of $\tilde{H}$ just after the second pulse is equal to the population in the corresponding eigenstate of H. In the adiabatic procedure, the t_1 and t_2 eigenstates with the highest energy are identified, as are the states with the lowest energy. The same procedure is used to connect populations and coherences from the basis of eigenstates of $\tilde{H}$ to the basis defined by H' just before the arrival of the third laser pulse.

In the basis of $\tilde{H}$, second-order perturbation theory leads to a Redfield equation for the time evolution of the reduced density matrix during t_2,

$$\frac{\mathrm{d}}{\mathrm{d}t}\sigma_{v'u'}(t) = -i\omega_{v'u'}\sigma_{v'u'}(t) + \sum_{vu} R_{v'u'vu}\sigma_{vu}(t). \tag{16}$$

Here, $\omega_{v'u'} = E_{v'} - E_{u'}$ and the Redfield tensor is given by

$$R_{v'u'vu} = -\delta_{u'u}\sum_p \Gamma^+_{v'ppv} - \delta_{v'v}\sum_p \Gamma^-_{uppu'} + \Gamma^+_{uu'v'v} + \Gamma^-_{uu'v'v}. \tag{17}$$

The components of the Redfield tensor with $v'=u'$ and $v=u$ describe population redistribution. Components with $v'=v$ and $u'=u$ damp the coherence σ_{vu}. The other elements describe coherence transfer and coupling between populations and coherences. The gamma tensors that appear in Eq. (17) are given in terms of the system-bath interaction as

$$\Gamma^+_{v'u'll'} = \sum_{mnm'n'} \langle v'|b^\dagger_m b_n|u'\rangle\langle l|b^\dagger_{m'}b_{n'}|l'\rangle J_{mnm'n'}(\omega_{ll'}), \tag{18}$$

$$\Gamma^-_{v'u'll'} = \sum_{mnm'n'} \langle v'|b^\dagger_{m'} b_{n'}|u'\rangle\langle l|b^\dagger_m b_n|l'\rangle J^-_{mnm'n'}(\omega_{v'u'}). \tag{19}$$

Here, the spectral densities $J(\omega)$ give the effective phonon density at energy ω, i.e., the phonon density multiplied by the interaction strength with the system. They are defined by

$$J_{mnm'n'}(\omega) = \int_0^\infty \mathrm{d}t e^{i\omega t}\langle F_{mn}(t)F_{m'n'}(0)\rangle, \tag{20}$$

$$J^-_{mnm'n'}(\omega) = \int_0^\infty \mathrm{d}t e^{i\omega t}\langle F_{m'n'}(0)F_{mn}(t)\rangle, \tag{21}$$

where the brackets $\langle\cdots\rangle$ denote quantum mechanical correlation functions at finite temperature. Because of the assumption that the bath is harmonic, the spectral densities can be evaluated explicitly as

$$J_{mnm'n'}(\omega) = \pi\sum_x g^x_{mn}g^x_{m'n'}(n_T(\omega_x)\delta(\omega+\omega_x) + (1+n_T(\omega_x))\delta(\omega-\omega_x)), \tag{22}$$

$$J^-_{mnm'n'}(\omega) = J_{mnm'n'}(-\omega), \tag{23}$$

with $n_T(\omega) = 1/(\exp(\omega/kT)-1)$ the Bose-Einstein distribution at temperature T.

The system-bath coupling strengths g^x_{mn} in Eq. (22) determine the effect of a bath mode with frequency ω_x on the

matrix element $\tilde{H}_{mn}$. In order to model these, we assume that we have some information on the classical auto- and cross-correlation functions,

$$C_{mnm'n'}(t) = \langle \Delta H_{mn}(t) \Delta H_{m'n'}(0) \rangle_{\mathrm{CL}}. \tag{24}$$

The brackets $\langle \cdots \rangle_{\mathrm{CL}}$ describe a classical average and ΔH_{mn} are the fluctuations in the matrix elements of the Hamiltonian in the fixed basis. These correlation functions can be obtained from a molecular dynamics simulation, or a model form can be used. The classical correlation functions describe how the matrix elements of the system Hamiltonian fluctuate in time. These classical fluctuations describe the same physics as the quantum mechanical coupling strengths g and are used to determine these couplings in the current method.

In order to replace the quantum correlation function in Eq. (20) with this classical correlation function we use the relation described in Refs. 41 and 42. The Fourier transform of the classical correlation function is given by

$$J^{C}_{mnm'n'}(\omega) = \int_0^\infty dt e^{i\omega t} C_{mnm'n'}(t)$$

$$= \frac{\pi kT}{|\omega|} \sum_q g^x_{mn} g^x_{m'n'} \delta(\omega_q - |\omega|). \tag{25}$$

Comparing this with the quantum mechanical result [Eq. (22)] one observes that

$$J_{mnm'n'}(\omega) = \frac{|\omega|}{kT} (n_T(|\omega|)\Theta(\omega)$$

$$+ (1 + n_T(|\omega|))\Theta(-\omega)) J^{C}_{mnm'n'}(\omega). \tag{26}$$

From the symmetries of the classical correlation function, we find that

$$\Gamma^{-}_{uvv'u'} = \Gamma^{+}_{v'u'vu}, \tag{27}$$

and we see from Eq. (18) that the Γ^+ tensor is symmetric in its first two indices. With these two results, the Redfield tensor simplifies to

$$R_{v'u'vu} = -\delta_{u'u} \sum_p \Gamma^{+}_{v'ppv} - \delta_{v'v} \sum_p \Gamma^{+}_{u'ppu} + \Gamma^{+}_{u'uv'v}$$

$$+ \Gamma^{+}_{v'vu'u}. \tag{28}$$

This equation, together with Eqs. (18), (25), and (26), expresses the Redfield tensor in terms of the classical correlation functions. From this, the relaxation tensor follows as the solution to Eq. (16),

$$\mathcal{R}_{v'u'vu}(t_2) = (e^{(-i\Omega + R)t_2})_{v'u'vu}, \tag{29}$$

with $\Omega_{v'u'vu} = \omega_{vu}\delta_{v'v}\delta_{u'u}$ and R the Redfield tensor.

IV. RESULTS

We demonstrate our approach by applying it to NMA, a molecule that contains a single peptide bond and is often used as a model for the protein unit. In particular, the infrared spectroscopy of this molecule has been studied well.[5,12,17,25–27,30,31,43] In this section, we describe the fluctuations in the amide-1 and amide-2 frequencies and the coupling between these two modes in NMA, followed by a discussion of our simulated infrared spectra.

A. Fluctuations

To describe the vibrational states in the amide group, we need to distinguish between the fixed basis states in which we write down the Hamiltonian [Eq. (1)] and the fluctuating eigenstates of this Hamiltonian. We will use the notation amide-1 and amide-2 for the fixed basis states. They have fluctuating frequencies and are coupled through a bilinear interaction term that is also time dependent. The eigenstates in each realization of the disorder (the $|u\rangle$, $|u'\rangle$, $|v\rangle$ and $|v'\rangle$ states in Sec. II), which are visible in the spectrum and used in the theory of Redfield relaxation, are denoted amide-I and amide-II.

In order to obtain the classical correlation functions $C_{mnm'n'}$, $(m,n,m',n' \in 1,2)$, we have performed density functional (DFT) calculations and molecular dynamics (MD) simulations of NMA in D_2O (details will be published elsewhere[44]). The DFT calculations are used to parametrize a map that relates the amide-1 and amide-2 frequencies and the interaction between them to electrostatic properties of the environment. With this map the time dependent environment (in particular the fluctuating positions of partial charges in the solvent) can be translated into trajectories for the two frequencies and the coupling. This method is an extension of the work described in Ref. 31 to include the amide-2 mode. Histograms obtained from 1 ns trajectories for the amide-1 and amide-2 frequencies and the coupling are shown in Fig. 3. The figure demonstrates that the fluctuations in all three parameters are almost completely Gaussian.

With the assumption that the stochastic process of these fluctuations is indeed Gaussian, we use auto- and cross-correlation functions calculated from the frequency and coupling trajectories as the input for our simulations. The two autocorrelation functions for the amide-1 and amide-2 energies and the cross-correlation function between these energies are shown in Fig. 4(a). The correlation functions that involve the fluctuations in the coupling are shown in Fig. 4(b). The Fourier transforms of the correlation functions—the classical spectral densities—are shown in Figs. 4(c) and 4(d). They show how effectively available bath modes influence frequencies and couplings in the system.

The autocorrelation functions show a rapid memory loss for all parameters. This initial loss of correlation is followed by beating in the amide-1 frequency, caused by vibrations in the hydrogen bond between the amide oxygen and the solvent. This effect is not seen in the coupling, while it is weak in the amide-2 mode. Because the amide-2 mode is farther away from the solvent molecules than the amide-1, this is what we would expect from an electrostatic NMA-solvent interaction. Furthermore, we observe from Fig. 4(a) that the amide-1 and amide-2 frequencies are anticorrelated, as expected from the resonant valence bond in the amide group (Fig. 1).[45] The frequencies of the eigenstates (amide-I and amide-II) are also anticorrelated, and we find the correlation factor between them to be −0.50. The anticorrelation that we

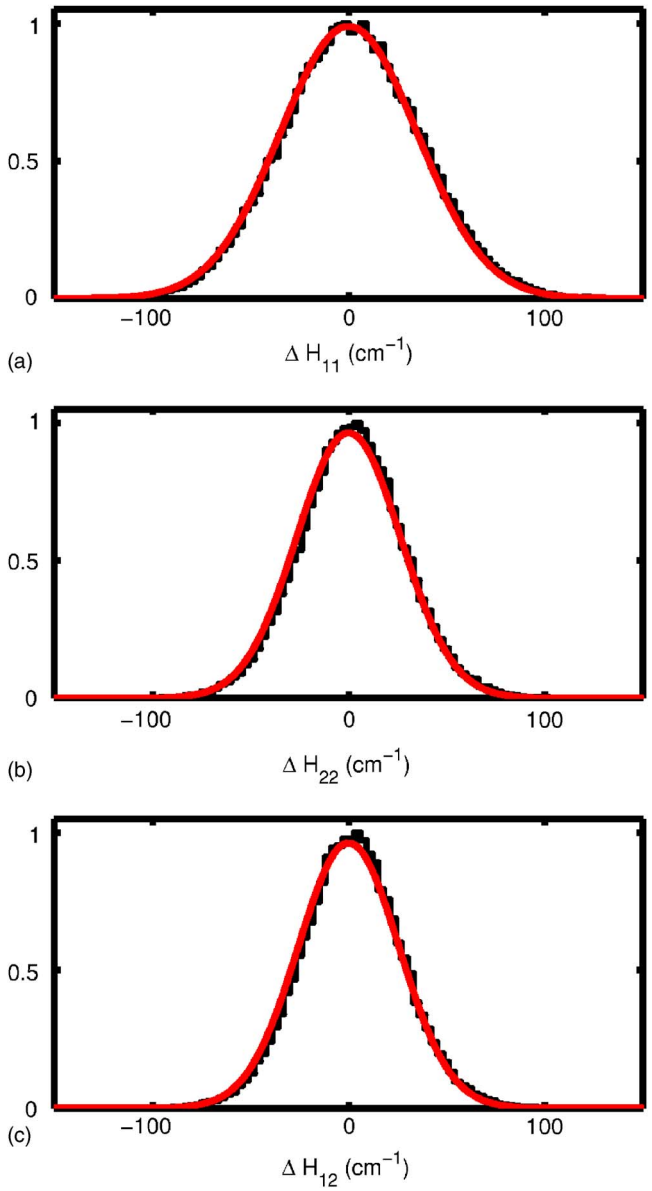

FIG. 3. (Color online) Histograms of the fluctuations in the (a) amide-1 frequency, (b) amide-2 frequency, and (c) coupling obtained from the molecular dynamics trajectory. The solid lines are Gaussian functions; their widths are equal to the standard deviations calculated from the trajectories.

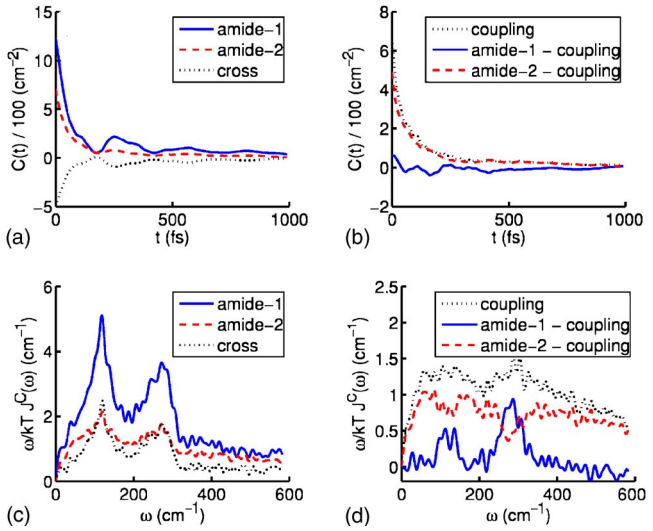

FIG. 4. (Color online) Correlation functions and spectral densities for the system parameters, obtained using an electrostatic map in combination with molecular dynamics simulations (Ref. 44). Panel (a) shows the autocorrelation functions for the amide-1 and amide-2 frequencies and the cross-correlation function between these two parameters. Panel (b) shows the correlation functions that involve the coupling. Panels (c) and (d) show the corresponding spectral densities.

find is much larger than the −0.28 measured in dimethyl sulfoxide (DMSO) (Ref. 45) and also larger than the value of −0.16 found in a calculation on NMA in H_2O.[26] From Fig. 4(b), the coupling and the amide-2 frequency appear to be strongly correlated, while the correlation between the amide-1 mode and the coupling is almost zero. This suggests that there is a second effect in the NMA structure or the solvent that influences the amide-2 frequency, but has no effect on amide-1.

The rate of energy transfer between the amide-I and amide-II mode is directly proportional to the value of the spectral density at the energy gap between the two modes. As shown in Fig. 4, the spectral density for the amide-1 mode has a clear peak near 110 cm^{-1}. This peak is caused by vibrations in the hydrogen bond between oxygen in the amide group and the solvent. The mode is similar to a mode observed in liquid D_2O at 170–180 cm^{-1}.[46,47] In our case the frequency is somewhat lower, as should be expected from the mass difference between NMA and D_2O. The presence of a resonance close to the energy gap between amide-I and amide-II modes in our simulation lends further support to the suggestion by Wang and Hochstrasser[48] that solvent modes play an important role in the relaxation process.

The relaxation rate between the amide-I and the amide-II modes is not only determined by the fluctuations described above, but also depends on the average coupling and on the difference between the average amide-1 and amide-2 energies. For a calculation of the (nonlinear) infrared spectra, we furthermore need the anharmonicities and transition dipoles. In principle, all these parameters follow from the MD trajectories combined with the DFT map. It is known, however, that frequencies obtained in DFT calculations may not be completely accurate; they often need to be corrected by a few percent.[49] Therefore, we have treated the difference between the amide-1 and amide-2 frequencies as an adjustable parameter and have chosen its value $\Delta E = H_{S,11} + \langle H_{SB,11}\rangle - H_{S,22} - \langle H_{SB,22}\rangle$ such that $\sqrt{(\Delta E)^2 + 4\langle H_{SB,12}\rangle^2}$ reproduces the experimental gap of 100 cm^{-1} between the amide-I and amide-II modes.[12] Here, $\langle H_{SB,12}\rangle$ is the average coupling obtained from our MD simulation. Its value of 24 cm^{-1} implies that we take $\Delta E = 88$ cm^{-1}. In the calculation of the spectra, we use an amide-2 dipole that has a length of 0.77 times the amide-1 dipole; the angle between the two dipoles is 64°. These values, obtained by averaging the DFT map over our MD trajectory, compare favorably with the values of 0.6 and 75° reported from a fit to the experimental spectrum.[12] Anharmonicities are taken to be 16 cm^{-1} (Ref. 5) for the amide-1 and 11 cm^{-1} (Ref. 12) for the amide-2 mode. The temperature is 300 K.

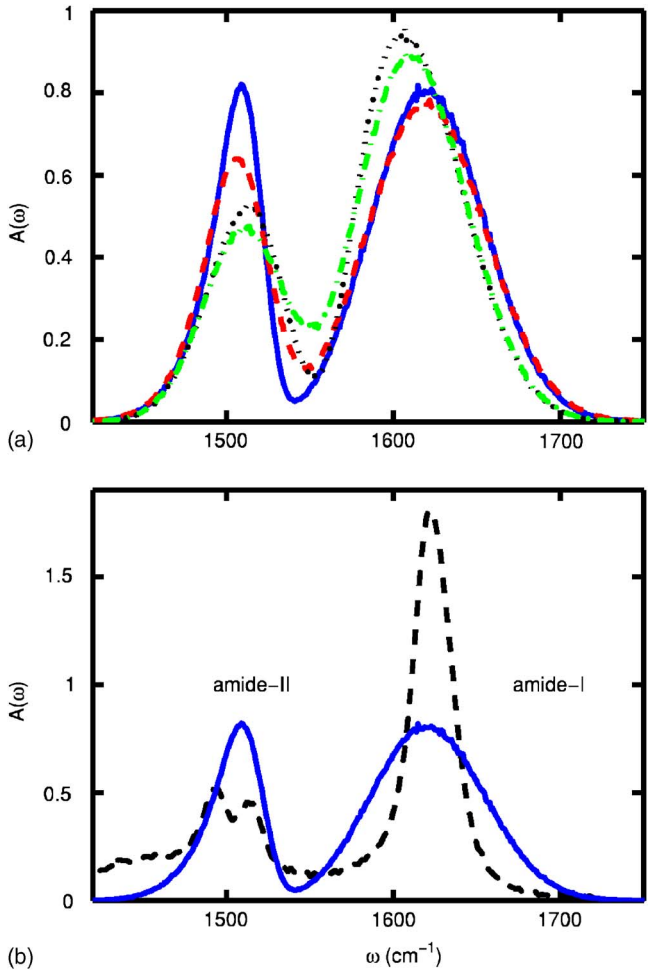

FIG. 5. (Color online) Calculated spectra [panel (a)] obtained from the full calculation (solid line), and from three simplified models: neglecting anticorrelation between the fluctuations in the amide-1 and amide-2 frequencies (dashed line), neglecting fluctuations in the coupling (dotted line), and neglecting both the anticorrelation between the amide-1 and amide-2 fluctuations and the fluctuations in the coupling (dash-dotted line). Panel (b) shows the full calculation (solid line) together with the experimental spectrum from Ref. 12 (dashed line). All spectra are normalized to the same integrated intensity.

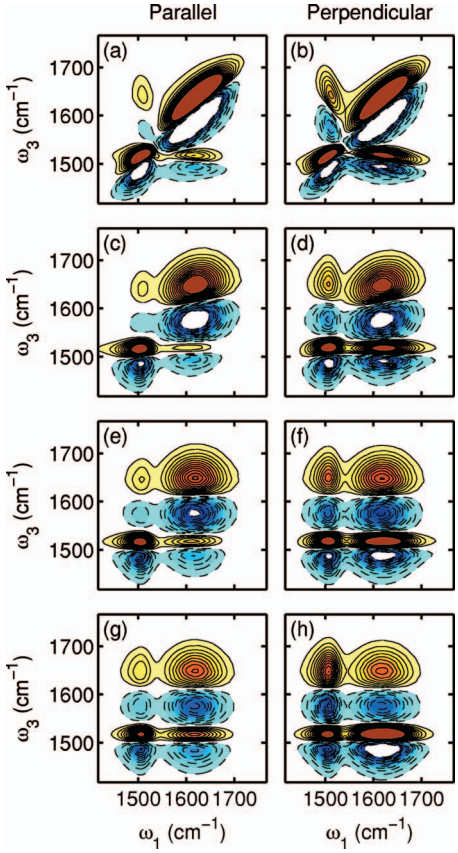

FIG. 6. (Color) Calculated 2DIR spectra for [(a) and (b)] $t_2=10$ fs, [(c) and (d)] 80 fs, [(e) and (f)] 400 fs, and [(g) and (h)] 2000 fs. 26 Equidistant contours were drawn from −60% to +60% of the maximum in the 80 fs spectrum. Solid contours filled with red and yellow show the bleaching and stimulated emission peaks; induced absorption peaks are plotted in blue with dashed contours.

B. Spectra and relaxation

Our model includes fluctuations in the frequencies of the amide-1 and amide-2 modes, fluctuations in the couplings, and correlations between these fluctuations. In order to understand their influence, we also simulated spectra omitting some of these effects. In particular, we performed simulations leaving out the fluctuations in the coupling, the anticorrelation between the two amide frequencies, and both. In Fig. 5(a), we present the resulting static linear spectra, together with the complete calculation. 2DIR spectra (not shown) give very similar information on the effects discussed here. It is clear that both the fluctuations in the coupling between fixed basis states and the anticorrelation between the amide frequencies have a strong effect on the spectrum. Both effects reduce the amplitude of the amide-I peak. Due to the nonlinear effect of the coupling on the eigenenergies, a fluctuating coupling has a larger effect on the eigenstates than a constant coupling equal to the average over the dynamics. The lower effective coupling reduces the frequency difference between the amide-I and amide-II eigenstates, visible in the spectrum as a blueshift of the amide-II peak and a redshift of the amide-I peak.

Because our approach neglects motional narrowing, we do not expect the line shape in the spectrum to be in good agreement with experiment. It is indeed clear from Fig. 5(b) that the peaks are narrower in experiment than in our simulations. The quantity that can be compared directly is the integrated peak intensity. The analysis of the experimental spectrum [Fig. 5(b)] is complicated by the presence of the Fermi resonance in the amide-II peak and by the tail at the red side of the spectrum. With the assumption that the Fermi resonance originates from interaction of the amide-II vibration with a completely dark mode, we assign all intensity between the local minima at $\omega=1424$ cm^{-1} and $\omega=1554$ cm^{-1} to amide-II and obtain an estimate for the experimental ratio of the amide-II intensity to the amide-I intensity of 0.51. We stress that this should be taken as a rough estimate. The relative intensity found in our complete simulation is 0.47, in good agreement with the experimental value.

The 2DIR spectra calculated as described in the previous section are shown in Fig. 6 for waiting times varying between 10 and 2000 fs. The spectra in the two columns have been calculated for respectively the ZZZZ polarization con-

dition, with all laser pulses polarized parallel, and for the ZZYY polarization, with the second pulse pair perpendicular to the first pair. The spectra have been convoluted with a two-dimensional Lorentzian line shape with a half width of 5 cm^{-1}. For short waiting time, fluctuations in the frequency are small and the frequency changes little from the first pulse pair to the second. This leads to a diagonally elongated peak, as is seen in Figs. 6(a) and 6(b). Memory is lost for longer waiting times. As the correlation between the frequency seen by the first pulse pair and that seen by the second pair disappears, the diagonal elongation disappears [Figs. 6(e)–6(h)].[11]

Cross peaks appear in the spectrum when two modes are coupled. Tilting of the cross peak away from the horizontal can occur because of frequency correlations between the two different modes that make the cross peak.[13] This is seen in our spectra for $t_2=10$ fs [Figs. 6(a) and 6(b)], where the cross peaks are tilted in the antidiagonal direction. This effect directly reflects the anticorrelation between the two amide mode frequencies. It was seen in the two-color experiment on NMA in DMSO by Rubtsov,[45] but is not clearly distinguishable in the Tokmakoff experiments in D_2O.[12] We also observe that for short t_2, the cross peak above the diagonal ($\omega_3>\omega_1$) shows up at higher ω_1 and lower ω_3 than expected from the positions of the two diagonal peaks. This effect can also be explained from the anticorrelation. If the amide-II frequency is high during t_1, the probability of having a low amide-I frequency during t_3 is large. As a result, the gap between the two modes is smaller than it is on average and therefore the coupling between them is more effective; i.e., the contributions of amide-1 to amide-II and of amide-2 to amide-I are large. This larger effective coupling gives rise to a stronger signal in the cross peak in the high ω_1 and low ω_3 region. The effect is increased by the positive correlation that exists between the amide-2 frequency and the coupling. At the other side of the cross peak (low ω_1, high ω_3), the effective coupling is small and the signal is therefore weak. The net effect is the observed shift of the cross peak. The shift disappears for longer t_2, because memory of the initial excitation frequency is lost and a high amide-II frequency during t_1 no longer implies a low amide-I frequency during t_3. The cross peak for longer waiting times thus appears at the expected position.

For these longer waiting times, dynamics during t_2 are expected to show up in the cross peaks because the relative populations of the two states that form the cross peak are changed. The relative intensity of the cross peak compared to the diagonal peaks increases if population transfer occurs. This effect is clearly observed in Fig. 6, especially in the perpendicular polarization. There, relaxation has a much larger effect on the spectra than in the all-parallel case, reflecting the fact that the dipoles of the modes in our model are almost perpendicular on average. Finite temperature causes downward relaxation to be faster than upward. The effect of this difference is that, with increasing waiting time, the low-energy diagonal peak and the cross peak below the diagonal gain amplitude compared to the other peaks.

In Fig. 7, the solid line shows the average population of the highest eigenstate (amide-I) as a function of waiting time, after initial excitation of amide-II. The population shown is the ensemble average of the population in the highest eigenstate of the Hamiltonian as a function of t_2. If we exclude coupling between populations and coherences (secular approximation), the Redfield equation reduces to a master equation for the populations, which can be solved to give

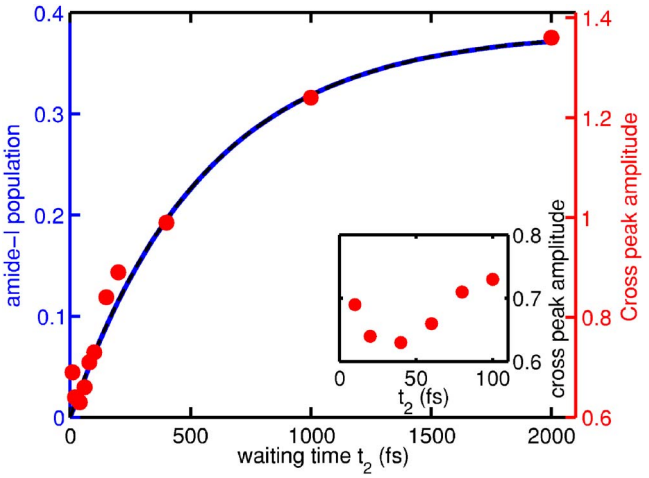

FIG. 7. (Color online) Amplitude of the bleaching part of the cross peak (dots) and calculated amide-I population following amide-II excitation (solid line). The cross peak amplitude was measured in the perpendicular polarization spectrum as the local maximum in a slice at ω_1 equal to the maximum of the amide-II peak ($\omega_1=1507$ cm^{-1}). The inset shows the cross peak intensity for short waiting times. The dashed line is a fit of the amide-I population to Eq. (30), which hardly deviates from the calculated population.

$$P_I(t) = P_I^{\mathrm{eq}}(1 - e^{-t/\tau}). \tag{30}$$

A fit of the population to this model, plotted in Fig. 7 as a dashed line (which is hardly distinguishable from the solid line), gives very good agreement. The value for P_I^{eq} follows from the gap between the two eigenstates of the average Hamiltonian. This gap is $\omega=\sqrt{(\Delta E)^2+4\langle H_{SB,12}\rangle^2}=100$ cm^{-1}, leading to $P_I^{\mathrm{eq}}=1/(1+\exp(\omega/kT))=0.38$. The best fit parameter for the relaxation time is $\tau=560$ fs. This time scale seems very reasonable, given the known overall decay time of the amide-I mode of 450 fs,[5] and the fact that we did not include relaxation to other modes. Note that in the present model the sum of amide-I and amide-II population is constant, so the relaxation time scale is the same for both modes.

Also shown in Fig. 7 is the amplitude of the bleaching part of the upper cross peak (filled dots). Here, the amplitude is defined as the local maximum in a slice at ω_1 equal to the maximum of the amide-II peak ($\omega_1=1507$ cm^{-1}). We plot the amplitude in the perpendicular polarization, because in this polarization geometry the two almost perpendicular amide modes produce an intense cross peak signal. The exact value of the cross peak amplitude as a function of time is determined by the relaxation, shifts of peak positions, and changing line shapes. To single out the effect of relaxation, we estimate the resulting enhancement in cross peak intensity between $t_2=0$ and t_2 much longer than the relaxation time. For two eigenstates with perpendicular dipoles we find, in the secular approximation and ignoring fluctuations, an enhancement factor equal to $8(1+P_I^{\mathrm{eq}})/7$. With an equilibrium

value of the amide-I population of $P_I^{eq}=0.38$ the factor is 1.6, smaller than the value obtained from our simulated spectra (enhancement factor 2). Thus, the cross peak grows faster than expected from the influence of vibrational relaxation. Nevertheless, we observe from Fig. 7 that the change in the cross peak amplitude gives a reasonable estimate of the population transfer.

The effect of population transfer on the cross peak amplitude is included in the stimulated emission contribution to the nonlinear signal. Pathways with a population during t_2 give rise to an increase of the amplitude as population is transferred from the amide-II to the amide-I state. In the other stimulated emission pathway that shows up in the cross peak, the system is in a coherent superposition of the two one-quantum states. Due to inhomogeneous dephasing, this contribution decays quickly, which is responsible for the initial decay of the cross peak amplitude seen in the inset in Fig. 7. The third contribution to the cross peak comes from the ground state bleach diagram, and is constant in time.

The first of three effects that affect the cross peak amplitude through changes in line shapes and in interference is the shift of both positive and negative parts of the cross peak in the $(-\omega_1,+\omega_3)$ antidiagonal direction, explained earlier. Because we defined amplitude as the maximum in a slice at a fixed value of ω_1, the peak shift changes the amplitude. A second effect that increases the amplitude originates from reduced interference with the induced absorption part of the cross peak. The induced absorption contribution that is present at $t_2=0$ originates from the coherence between the combination state and the amide-II state and decays due to relaxation. At the same time, a new contribution from the coherence between the amide-I overtone and the amide-I state becomes possible. This new peak appears at a value of ω_3 that is 11 cm^{-1} lower than the original one. The induced absorption part of the cross peak thus shifts to lower ω_3 with increasing waiting time. The shift reduces the interference with the bleaching and stimulated emission peaks, which therefore increase in amplitude. Finally, the amplitude of the cross peak is influenced by the changes in line shape from a narrow antidiagonal peak at short t_2 to a broader two-dimensional Gaussian for long t_2. Apart from the direct decrease of the amplitude when broadening occurs, the line shape determines the amount of interference between the positive and negative parts of the cross peak and thereby changes the amplitude.

To conclude this section, we note that no coherent oscillations in the calculated population are observed, because Fig. 7 shows the population in the amide-I state. The population in the amide-1 basis state would show such oscillations. These are caused by the fact that the amide-1 state is not an eigenstate of the system Hamiltonian. Population is transferred coherently between amide-1 and amide-2 as a consequence of the interaction between these two modes.

V. CONCLUSION

In summary, we have used Redfield theory to include vibrational relaxation in the simulation of two-dimensional infrared spectra. In our description, system modes are coupled by a bilinear interaction term that can be arbitrarily large. The coupling between system and bath modes is obtained from classical correlation functions. The effect of fluctuations on the line shape is treated by a stochastic model for vibrational frequencies and couplings. This model can account for arbitrary correlations between the frequencies and couplings, as long as the fluctuations are Gaussian. The model does not include motional narrowing. 2DIR spectra can be calculated for different polarization directions using the standard nonlinear response formalism.

We have applied the model to the amide-I and amide-II vibrations in *N*-methylacetamide dissolved in heavy water. Using an electrostatic map in combination with molecular dynamics simulations, we have found that the fluctuations are indeed Gaussian, and we have obtained the required correlation functions. Both the correlation between fluctuations in the two frequencies and the fluctuations in the coupling have a large influence on the simulated spectra.

Vibrational relaxation, shifts in peak positions, and changing line shapes affect the intensity of the cross peaks in the 2DIR spectrum. We have shown that the cross peak amplitude gives a reasonable measure of the relaxation process. The relaxation between the amide-I and the amide-II modes is almost monoexponential, and takes place on a time scale of 560 fs, which is comparable to values found in experiment. The fact that fast relaxation takes place between amide-I and amide-II means that a full understanding of energy transport in proteins can only be obtained from models which explicitly include multiple vibrational modes. Our model does not include relaxation to other vibrational modes than amide-I or amide-II. Of course, this relaxation is present in experiment, where it leads to a decreasing intensity of all peaks in the spectrum for longer waiting times. It will be of interest to extend the method to describe relaxation to other vibrational modes, such as the amide-III mode, or to study relaxation in larger systems, such as peptides and proteins. Finally, the effect of motional narrowing on two-dimensional line shapes, especially in the cross peak region, needs more attention. Motional narrowing can be included with the phenomenological procedure outlined at the end of Sec. II, or by comparing the results described here with spectra obtained from numerical propagation of the Schrödinger equation.[14,23,24]

ACKNOWLEDGMENTS

The authors wish to thank Andrei Tokmakoff and Lauren DeFlores for discussions and for sharing experimental results. One of the authors (T.l.C.J.) acknowledges the Netherlands Organization for Scientific Research (NWO) for support through a VENI grant.

APPENDIX: GENERATING A CORRELATED GAUSSIAN RANDOM PROCESS

In this appendix, we explain the procedure we developed to generate a Gaussian random process for variables with arbitrary correlations. It allows us to calculate spectra for coupled states from given auto- and cross-correlation func-

tions of frequencies and couplings. The method is capable of treating any time scale in the correlation functions, as well as arbitrary cross correlations.

For the simulation of the 2DIR spectrum for N oscillators, we need N local mode energies H_{nn} and $\frac{1}{2}N(N-1)$ couplings H_{mn}, $n>m$, at time $t=0$ and at time $t=t_2$. We want to build a random process that satisfies the given correlation functions,

$$\langle \Delta H_{kl}(t)\Delta H_{mn}(t)\rangle = \langle \Delta H_{kl}(0)\Delta H_{mn}(0)\rangle = C_{klmn}(0), \quad \text{(A1)}$$

$$\langle \Delta H_{kl}(t)\Delta H_{mn}(0)\rangle = \langle \Delta H_{kl}(0)\Delta H_{mn}(t)\rangle = C_{klmn}(t), \quad \text{(A2)}$$

with $\Delta H_{ij}(t)=H_{ij}(t)-\langle H_{ij}\rangle$.

In total, for a given time t, we want to get $M=N(N+1)$ correlated random variables. These variables are constructed by applying a linear transformation $A(t)$ to a set $\{h_i;i=1\ldots M\}$ of uncorrelated Gaussian random variables with zero mean and standard deviation of 1. If we subtract the mean and order the correlated variables H_i in a vector in some way as

$$\Delta H = (\Delta H_1(0),\Delta H_2(0),\ldots,\Delta H_M(0),\Delta H_1(t),\ldots,\Delta H_M(t)), \quad \text{(A3)}$$

the linear transformation $A(t)$ can be written as a matrix $A_{ij}(t)$. The index i of a stochastic variable ΔH_i is now a multi-index, replacing a pair mn.

Applying the linear transformation to the correlation functions in Eqs. (A1) and (A2), we find

$$\langle \Delta H_i \Delta H_j\rangle = \left\langle \sum_{kl} A_{ik}h_k A_{jl}h_l \right\rangle = \sum_{kl} A_{ik}A_{jl}\langle h_k h_l\rangle = \sum_k A_{ik}A_{jk} =: \mathbf{A}_i\cdot\mathbf{A}_j. \quad \text{(A4)}$$

In the third step we used the uncorrelated nature of the h variables and in the last step we defined the vectors that form the columns of the A matrix. Comparison with Eq. (A1) gives constraints on these vectors

$$|\mathbf{A}_i|^2 = C_{i,i}(0),\ i\leqslant M, \quad \text{(A5)}$$

$$|\mathbf{A}_i|^2 = C_{i-M,i-M}(0), \quad i>M, \quad \text{(A6)}$$

$$\mathbf{A}_i\cdot\mathbf{A}_j = C_{i,j}(0), \quad i,j\leqslant M, \quad \text{(A7)}$$

$$\mathbf{A}_i\cdot\mathbf{A}_j = C_{i-M,j-M}(0), \quad i,j>M, \quad \text{(A8)}$$

$$\mathbf{A}_i\cdot\mathbf{A}_j = C_{i,j-M}(t), \quad i\leqslant M, j>M, \quad \text{(A9)}$$

$$\mathbf{A}_i\cdot\mathbf{A}_j = C_{i-M,j}(t), \quad i>M, j\leqslant M \quad \text{(A10)}$$

With these vector relations, it is easy to construct the required matrix A, for example by

$$A_{ij} = \frac{1}{A_{jj}}\left(\mathbf{A}_i\cdot\mathbf{A}_j - \sum_{k=1}^{j-1} A_{ik}A_{jk}\right), \quad 1\leqslant j<i \quad \text{(A11)}$$

$$A_{ii} = |\mathbf{A}_i|^2 - \sum_{k=1}^{i-1} A_{ik}^2. \quad \text{(A12)}$$

It is clear that the construction of this matrix is not unique. The required correlated variables are found by multiplying the matrix with a vector h containing uncorrelated Gaussian random variables[50] with zero mean and standard deviation 1.

[1] A. S. Davydov, *Solitons in Molecular Systems* (Reidel, Dordrecht, 1985).
[2] A. Laubereau and W. Kaiser, Rev. Mod. Phys. **50**, 607 (1985).
[3] H. Fujisaki and J. E. Straub, Proc. Natl. Acad. Sci. U.S.A. **102**, 6726 (2005).
[4] X. Yu and D. M. Leitner, J. Phys. Chem. B **107**, 1698 (2003).
[5] P. Hamm, M. Lim, and R. M. Hochstrasser, J. Phys. Chem. B **102**, 6123 (1998).
[6] N. Demirdöven, C. M. Cheatum, H. S. Chung, M. Khalil, J. Knoester, and A. Tokmakoff, J. Am. Chem. Soc. **126**, 7981 (2004).
[7] A. W. Smith and A. Tokmakoff, J. Chem. Phys. **126**, 045109 (2007).
[8] H. Maekawa, C. Toniolo, Q. Broxterman, and N. H. Ge, J. Phys. Chem. B **111**, 3222 (2007).
[9] S. Woutersen and P. Hamm, J. Chem. Phys. **115**, 7737 (2001).
[10] P. Mukherjee, A. T. Krummel, E. C. Fulmer, I. Kass, T. Arkin, and M. T. Zanni, J. Chem. Phys. **120**, 10215 (2004).
[11] M. Khalil, N. Demirdöven, and A. Tokmakoff, J. Phys. Chem. A **107**, 5258 (2003).
[12] L. P. DeFlores, Z. Ganim, S. F. Ackley, H. S. Chung, and A. Tokmakoff, J. Phys. Chem. B **110**, 18973 (2006).
[13] R. Venkatramani and S. Mukamel, J. Chem. Phys. **117**, 11089 (2002).
[14] T. L. C. Jansen, W. Zhuang, and S. Mukamel, J. Chem. Phys. **121**, 10577 (2004).
[15] W. Zhuang, D. Abramavicius, T. Hayashi, and S. Mukamel, J. Phys. Chem. B **110**, 3362 (2006).
[16] A. Ishizaki and Y. Tanimura, J. Chem. Phys. **125**, 084501 (2006).
[17] M. F. DeCamp, L. P. DeFlores, J. M. McCracken, A. Tokmakoff, K. Kwac, and M. Cho, J. Phys. Chem. B **109**, 11016 (2005).
[18] N. H. Ge, M. T. Zanni, and R. M. Hochstrasser, J. Phys. Chem. A **106**, 962 (2002).
[19] A. G. Dijkstra and J. Knoester, J. Phys. Chem. B **109**, 9787 (2004).
[20] S. Mukamel and D. Abramavicius, Chem. Rev. (Washington, D.C.) **104**, 2073 (2004).
[21] S. Mukamel, Phys. Rev. A **28**, 3480 (1983).
[22] J. Sung and R. J. Silbey, J. Chem. Phys. **115**, 9266 (2001).
[23] T. L. C. Jansen and J. Knoester, J. Phys. Chem. B **110**, 22910 (2006).
[24] H. Torii, J. Phys. Chem. A **110**, 4822 (2006).
[25] S. Ham, J. H. Kim, H. Lee, and M. H. Cho, J. Chem. Phys. **118**, 3491 (2003).
[26] T. Hayashi, W. Zhuang, and S. Mukamel, J. Phys. Chem. A **109**, 9747 (2005).
[27] T. Hayashi and S. Mukamel, J. Chem. Phys. **125**, 194510 (2006).
[28] H. Fujisaki, Y. Zhang, and J. E. Straub, J. Chem. Phys. **124**, 144910 (2006).
[29] P. Bour and T. A. Keiderling, J. Chem. Phys. **119**, 11253 (2003).
[30] J. R. Schmidt, S. A. Corcelli, and J. L. Skinner, J. Chem. Phys. **121**, 8887 (2004).
[31] T. L. C. Jansen and J. Knoester, J. Chem. Phys. **124**, 044502 (2006).
[32] S. Woutersen, R. Pfiser, P. Hamm, Y. Mu, S. Kosov, and G. Stock, J. Chem. Phys. **117**, 6833 (2002).
[33] N. G. Mirkin and S. Krimm, J. Mol. Struct. **377**, 219 (1996).
[34] S. Mukamel, *Principles of Nonlinear Optical Spectroscopy* (Oxford University Press, Oxford, 2005).
[35] D. M. Jonas, Annu. Rev. Phys. Chem. **54**, 425 (2003).
[36] V. May and O. Kühn, *Charge and Energy Transfer Dynamics in Molecular Systems* (Wiley, Berlin, 2000).
[37] C. M. Cheatum, A. Tokmakoff, and J. Knoester, J. Chem. Phys. **120**, 8201 (2004).
[38] R. M. Hochstrasser, Chem. Phys. **266**, 273 (2001).
[39] G. C. Schatz and M. A. Ratner, *Quantum Mechanics in Chemistry* (Dover, New York, 2002).
[40] A. G. Redfield, Adv. Magn. Reson. **1**, 1 (1966).

[41] J. S. Bader and B. J. Berne, J. Chem. Phys. **100**, 8359 (1994).
[42] J. L. Skinner, J. Chem. Phys. **107**, 8717 (1997).
[43] T. M. Watson and J. D. Hirst, Mol. Phys. **103**, 1531 (2005).
[44] R. Bloem, A. G. Dijkstra, T. I. C. Jansen, and J. Knoester (unpublished).
[45] I. V. Rubtsov, J. Wang, and R. M. Hochstrasser, Proc. Natl. Acad. Sci. U.S.A. **100**, 5601 (2003).
[46] E. W. Castner, Jr., Y. J. Chang, Y. C. Chu, and G. E. Walrafen, J. Chem. Phys. **102**, 653 (1995).
[47] C. J. Fecko, J. D. Eaves, J. J. Loparo, A. Tokmakoff, and P. L. Geissler, Science **301**, 1698 (2003).
[48] J. Wang and R. M. Hochstrasser, J. Phys. Chem. B **110**, 3798 (2006).
[49] F. Jensen, *Introduction to Computational Chemistry* (Wiley, Chicester, 1999).
[50] W. H. Press, S. A. Teukolsky, W. T. Vetterling, and B. P. Flannery, *Numerical Recipes in C++: the Art of Scientific Computing* (Cambridge University Press, 2002).